Environmental Science & Technology

Article

pubs.acs.org/est

Mechanisms and Kinetics of Alkaline Hydrolysis of the Energetic Nitroaromatic Compounds 2,4,6-Trinitrotoluene (TNT) and 2,4-Dinitroanisole (DNAN)

Alexandra J. Salter-Blanc,[†] Eric J. Bylaska,[‡] Julia J. Ritchie,[†] and Paul G. Tratnyek*,[†]

[†]Division of Environmental and Biomolecular Systems, Oregon Health & Science University, 20000 NW Walker Road, Portland, Oregon 97006, United States

[‡]William R. Wiley Environmental Molecular Sciences Laboratory, Pacific Northwest National Laboratory, P.O. Box 999, Richland, Washington 99352, United States

Supporting Information

ABSTRACT: The environmental impacts of energetic compounds can be minimized through the design and selection of new energetic materials with favorable fate properties. Building predictive models to inform this process, however, is difficult because of uncertainties and complexities in some major fate-determining transformation reactions such as the alkaline hydrolysis of energetic nitroaromatic compounds (NACs). Prior work on the mechanisms of the reaction between NACs and OH^- has yielded inconsistent results. In this study, the alkaline hydrolysis of 2,4,6-trinitrotoluene (TNT) and 2,4-dinitroanisole (DNAN) was investigated with coordinated experimental kinetic measurements and molecular modeling calculations. For TNT, the results suggest reversible formation of an initial product, which is likely either a Meisenheimer complex or a TNT anion formed by abstraction of a methyl proton by OH^-. For DNAN, the results suggest that a Meisenheimer complex is an intermediate in the formation of 2,4-dinitrophenolate. Despite these advances, the remaining uncertainties in the mechanisms of these reactions—and potential variability between the hydrolysis mechanisms for different NACs—mean that it is not yet possible to generalize the results into predictive models (e.g., quantitative structure−activity relationships, QSARs) for hydrolysis of other NACs.

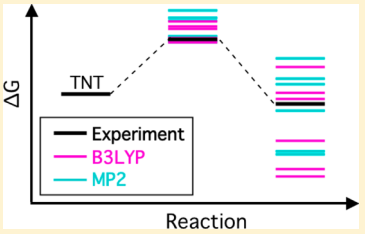

INTRODUCTION

Environmental release of energetic munitions compounds—through manufacture, handling, use (including in testing and training), and disposal—leads to potentially problematic contamination of soils, sediments, and water.[1,2] As new energetic materials and formulations are developed, however, their environmental impacts can be minimized through careful design and selection according to the principles of green chemistry.[3−5] A principle of green chemistry is that the design or selection of new substances should favor chemicals with limited environmental persistence and degradation products that are relatively benign.[3]

Achieving this goal—for energetic compounds or other chemicals—requires a sufficient understanding of chemical transformation pathways and kinetics to predict environmental fate. Obtaining the necessary chemical property data for this is a long-standing challenge, in part because the continuously expanding, large, and diverse population of chemicals of environmental concern precludes direct, empirical measurement of more than a small fraction of the data at a reasonable monetary and temporal cost.[6−8] This challenge has led to a great deal of interest in predictive models that can estimate contaminant fate properties efficiently and reliably.[6,8,9]

A common approach for predicting chemical properties employs empirical correlations such as linear free energy relationships (LFERs) and quantitative structure-activity relationships (QSARs). These models are obtained by calibration using training sets of response (target) variable data that are usually experimental and descriptor variable data that are relatively accessible. Such models are widely used as tools for predicting descriptors related to environmental fate and transport for use in regulatory decision-making and experimental prioritization.[6,8,9] In the case of (novel) energetic compounds, however, the challenge of obtaining experimentally determined environmental fate properties for model calibration is greatly increased by factors that are nearly unique to this type of material: (*i*) access to many of the materials is highly restricted, (*ii*) few environmental laboratories are equipped to perform experiments with such materials, and (*iii*) novel materials of this type are rarely prepared in sufficient quantities for environmental fate property testing.

In principle, the challenge of obtaining response variable data such as rate constants for model calibration can be overcome by determining the values from first principles (i.e., using molecular modeling). Given an understanding of the environmental fate mechanisms for a given family of compounds,

Special Issue: Rene Schwarzenbach Tribute

Received: October 31, 2012
Revised: January 18, 2013
Accepted: February 4, 2013
Published: February 4, 2013

reactions of novel compounds within this family can be modeled computationally to determine activation parameters for the reactions. According to the principles of transition state theory, these activation parameters can then be used to calculate rate constants for the reactions.[10] The result would be a correlation calibrated fully *in silico*, which could then be validated with obtainable experimental data for energetic (and model nonenergetic) compounds.

One family to which this method might be applied is energetic nitroaromatic compounds (NACs). The most familiar member of this group is 2,4,6-trinitrotoluene (TNT), which has long been used in a variety of energetic materials. Also included is a shock-insensitive alternative to TNT, 2,4-dinitroanisole (DNAN),[11] which is used in modern munitions formulations such as PAX-21.[12] While TNT and DNAN comprise a subfamily of substituted nitrobenzenes, other NACs used in emerging munitions formulations include substituted heterocycles, such as 5-nitro-1,2,4-triazol-3-one (NTO)—another insensitive replacement for TNT that is used in emerging munitions formulations[11]—and polyaromatic compounds. A representative sample of energetic NACs is shown in Figure 1; these and many more have been described previously.[13,14]

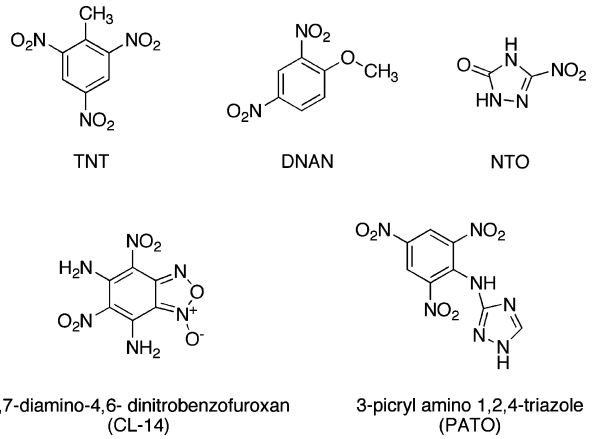

Figure 1. A selection of energetic NACs included or considered for use in munitions formulations.

The main abiotic transformation processes influencing the environmental fate of NACs in groundwater are reduction and alkaline hydrolysis.[15] While the pathways and kinetics associated with the reduction of NACs have been studied extensively, e.g., refs 16−20, the pathways associated with alkaline hydrolysis are not well characterized, despite considerable proof-of-concept testing of this process for engineered remediation of TNT-contaminated wastewaters.[21−31] In the case of TNT, there are significant inconsistencies in the experimental data, which likely arise from the sensitivity of the reaction to the nature of the solvent,[32,33] difficulty observing products in water due to their poor solubility,[26] and the influence of the concentration ratio between TNT and base on product distribution.[32,33] Previous computational studies of TNT reaction energetics have also failed to definitively determine the pathways of its reaction with OH^-.[34−36]

This incomplete understanding of the mechanisms of TNT hydrolysis in natural and engineered systems inhibits the prediction of degradation properties of future energetic NACs through the use of correlations calibrated with data determined fully in silico. Our goal in this paper is to clarify the mechanisms of TNT degradation by OH^- in water by taking a combined approach that emphasizes reconciliation of both experimental and computational data. An analysis of the kinetics of TNT disappearance in the presence of OH^- is presented and used to determine the experimental activation free energies ($\Delta G^{\ddagger}$) and reaction free energies (ΔG_{rxn}) for the processes. Also presented are $\Delta G^{\ddagger}$ and ΔG_{rxn} values for possible mechanisms of TNT degradation determined using molecular modeling. The measured and modeled results are then compared to assess which mechanisms predominate. Also reported is an analogous analysis for DNAN, which is structurally similar to TNT.

EXPERIMENTAL SECTION

Reagents. Stock solutions of NACs were prepared by dissolving solid-phase TNT (ChemService, Inc.; West Chester, PA) or DNAN (Alfa Aesar; Ward Hill, MA) in HPLC-grade acetonitrile (Fisher Scientific; Waltham, MA) to achieve a concentration of 10 g/L. All deionized (DI) water used was obtained from a Milli-Q system (EMD Millipore; Billerica, MA). HPLC mobile-phase components consisted of DI water and HPLC-grade methanol (Fisher Scientific; Waltham, MA). Phosphate buffers were prepared from sodium phosphate (mono- and dibasic) (Fisher Scientific; Waltham, MA) and adjusted with NaOH (Aldrich; St. Louis, MO) to pH 11.0, 11.7, and 12.0. Acidified acetonitrile was prepared by adding sufficient sulfuric acid to HPLC-grade acetonitrile to neutralize an equal volume of corresponding buffer.

Batch Experiments. Batch experiments were carried out in 20-mL amber VOA vials capped with Teflon-lined silicon septa (SUN Sri; Rockwood, TN). Each vial initially contained 20 mL of phosphate buffer (50 mM) at pH 11.0, 11.7, or 12.0. Vials were temperature equilibrated in water baths or in a cold room to 11.0, 25.0, 40.0, 55.0, or 65.0 °C. After temperature equilibration, TNT or DNAN was introduced to the reaction vial by injecting 200 μL of a 10-g/L stock solution prepared in acetonitrile (reaction initiation). Following introduction of TNT or DNAN, the vials were shaken by hand for ∼1 min (in the water bath) to ensure proper mixing. 1-mL aliquots were removed at specified times and quenched by mixing with an equal volume of acidified acetonitrile.

Quenched aliquots were analyzed by high-pressure liquid chromatography (HPLC). The HPLC setup included a Varian ProStar 210 solvent delivery module, 410 autosampler, and 330 photodiode array detector, with a Platinum C18 5 μ 250-mm × 4.6-mm column (Grace; Deerfield, IL). The mobile phase consisted of 1:1 DI water:methanol and was pumped at a flow rate of 1 mL min^{-1}.

Kinetic Modeling. The kinetics of TNT disappearance were fit assuming the reaction proceeds by a sequence of reversible and irreversible steps

$$\mathrm{TNT} + \mathrm{OH}^- \underset{k_{-1}}{\overset{k_1}{\rightleftharpoons}} \mathrm{P1} \xrightarrow{k_2} \mathrm{P2} \qquad \text{(Scheme 1)}$$

where P1 is the first product, P2 is the second product, k_1 is the second-order rate constant for the forward portion of the first reaction, k_{-1} is the rate constant for the reverse portion of the first reaction, and k_2 is the rate constant for the second reaction. The reaction was simplified by assuming constant hydroxide concentration in the buffered system and then treating the formation of P1 as a pseudo-first-order process

dx.doi.org/10.1021/es304461t | Environ. Sci. Technol. 2013, 47, 6790−6798

$$\mathrm{TNT} \underset{k_{-1}}{\overset{k_{1,obs}}{\rightleftharpoons}} \mathrm{P1} \xrightarrow{k_2} \mathrm{P2} \qquad \text{(Scheme 2)}$$

where $k_{1,obs}$ is the observed pseudo-first-order rate constant for formation of P1.

Rate constants were determined by fitting concentration vs time data for TNT. The data were fit by simultaneous numerical solution to the following differential equations (eq 1 and eq 2) using IGOR Pro (Wavemetrics; Lake Oswego, OR).

$$\frac{d[\mathrm{TNT}]}{dt} = -k_{1,obs}[\mathrm{TNT}] + k_{-1}[\mathrm{P1}] \qquad (1)$$

$$\frac{d[\mathrm{P1}]}{dt} = k_{1,obs}[\mathrm{TNT}] - k_{-1}[\mathrm{P1}] - k_2[\mathrm{P1}] \qquad (2)$$

Data sets obtained at different pH values but at the same temperature were fit globally (i.e., simultaneously) to obtain values of $k_{1,obs}$ and [TNT] for each pH condition and single, global values for each k_{-1} and k_2 (as these are pH-independent values according to Scheme 1).

DNAN disappearance was fit to a simple, irreversible pseudo-first-order model as described in Scheme 3 and Scheme 4

$$\mathrm{DNAN} + \mathrm{OH^-} \xrightarrow{k_1} \mathrm{P} \qquad \text{(Scheme 3)}$$

$$\mathrm{DNAN} \xrightarrow{K_{1,obs}} \mathrm{P} \qquad \text{(Scheme 4)}$$

where P is the product of the reaction, k_1 is the second-order rate constant, and $k_{1,obs}$ is the observed pseudo-first-order rate constant. The data was fit to a pseudo-first-order model to obtain $k_{1,obs}$.

Plots of $k_{1,obs}$ vs [OH^-] (Supporting Information (SI), Tables S1 and S3) for both TNT and DNAN confirmed that the forward reactions characterized by $k_{1,obs}$ were pseudo-first-order with respect to [OH^-]. Given this, second-order rate constants, k_1, for TNT and DNAN were determined by linear regression to the $k_{1,obs}$ vs [OH^-] data for each temperature.

Molecular Modeling. In this study, the solution phase ΔG_{rxn} and $\Delta G^{\ddagger}$ were directly calculated from gas-phase reaction energy, entropy, and solvation energy differences using electronic structure calculations, continuum solvation models, and gas-phase entropy estimates. All calculations were performed using the NWChem program suite.[37] The electronic structure calculations were either performed using density functional theory (DFT)[38] with the B3LYP[39,40] exchange correlation potential or with second-order Møller−Plesset perturbation theory (MP2).[41] In all cases, the 6-311++G-(2d,2p) basis set was used (obtained from the Extensible Computational Chemistry Environmental Basis Set Database[42]). The solvation energies were estimated using the self-consistent reaction field theory of Klamt and Schüürmann (COSMO),[43] with the cavity defined by a set of overlapping atomic spheres with radii suggested by Stefanovich and Truong (H 1.172 Å, C- 2.096 Å, C= 1.635 Å, O 1.576 Å, and N 2.126 Å).[44] The dielectric constant of water used for all of the solvation calculations was 78.4. The solvent cavity discretization was generated from the surfaces of nonoverlapping spheres that were discretized by an iterative refinement of triangles starting from a regular octahedron. Three refinement levels, equivalent to 128 points per sphere, were used to define the solvent cavity in these calculations.

The geometries and harmonic frequencies for the reactants, products, and transition states were consistently optimized using the B3LYP calculation with COSMO. Transition states were determined for the Meisenheimer and proton abstraction reactions by performing constrained optimizations at a series of C−OH and CH−OH bond distances. The transition state for the S_N2 reactions were found by a quasi-Newton (BFGS) saddle point search initialized with d(C−OH) = 1.45 Å and d(C−NO_2) = 1.65 Å. The virtual entropies for each compound were estimated using formulas derived from statistical mechanics that are broken into translational, rotational, and frequency terms. In addition to the COSMO correction, cavitation and dispersion contributions to the solvation energy were added *a posteriori* using empirically derived expressions that depend only on the solvent accessible surface area. In this study, we used the parameterized formula given by Sitkoff et al.[45]

$$\Delta G_{cav+disp} = \gamma A + b \qquad (3)$$

where A is the solvent-accessible surface area, and γ and b are constants set to 5 cal mol^{-1} $Å^{-2}$ and 0.86 kcal mol^{-1}, respectively. Sitkoff et al. fit the constants γ and b to the experimentally determined free energies of solvation of alkanes[46] by using a least-squares fit.

RESULTS AND DISCUSSION

Formulation of Candidate Mechanisms. Generally, NACs can interact with bases (nucleophiles) to form charge-transfer complexes, radical anions, σ-complexes, or proton abstraction products.[47] Formation of σ-complexes has been observed from the interaction of various nucleophiles with a wide range of NACs.[48] σ-Complexes are formed as intermediates in the Ar−S_N mechanism of nucleophilic aromatic substitution.[11,49] This reaction involves reversible addition of a nucleophile to an electron-deficient carbon on an aromatic ring (in a rate determining step) followed by elimination of a leaving group from the same ring carbon.[48,49] In cases where this intermediate is stable enough to be isolated or detected, it is known as a Meisenheimer complex.[48−50] Stabilizing factors include the presence of electron withdrawing groups on the aromatic ring and poor leaving groups.[49] Meisenheimer complexes have been studied extensively;[48] however, most of these studies were performed in nonaqueous media, and evidence for this reaction occurring under environmentally relevant (natural and engineered) conditions is limited.

Of the prior studies that characterize the reaction of TNT and OH^- in water, several have hypothesized that a Meisenheimer complex is the initial product.[24,26,48] However, demonstrating the participation of this intermediate is difficult because of its short lifetime and limited solubility in water. The main evidence for its formation is from NMR spectra that were obtained while following the reaction in acetone (due to solubility constraints in water).[26] Whether these conclusions apply to aqueous media is uncertain, because other studies in nonaqueous or partially aqueous systems have shown that the initial product in the reaction of TNT with base is strongly influenced by the solvent.[32,33]

Alternatively, it has been suggested that direct nitro substitution could be the initial step in this reaction, based on NMR analysis of the final polymeric reaction products formed in water.[27] A third possible initial step is the abstraction of a methyl proton, which has been reported to form along with or instead of a Meisenheimer complex in nonaqueous or partially aqueous systems, possibly leading to the formation of a

Janovsky complex.[32,33] A recent theoretical study using DFT concluded that Meisenheimer-complex formation and/or proton abstraction are the most likely initial reactions in the interaction of TNT with OH^-.[34] All of the proposed initial steps for reaction between TNT and OH^- are summarized in Figure 2.

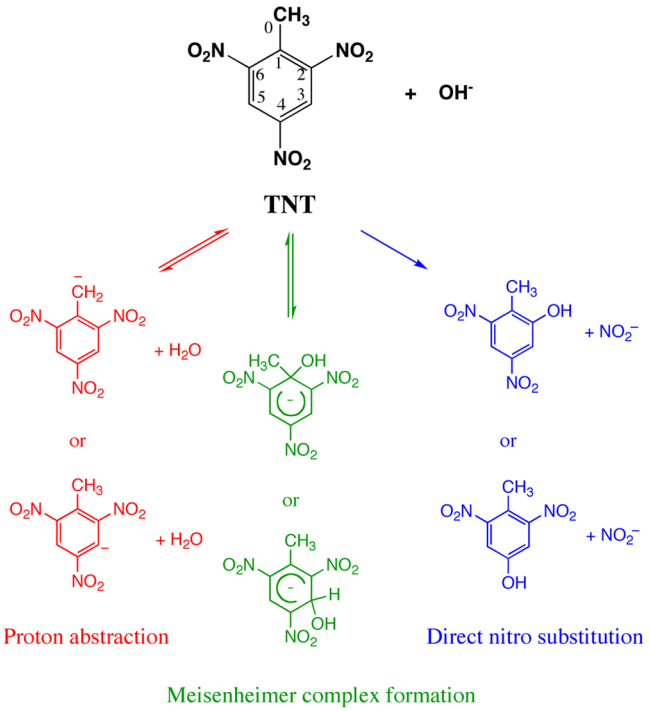

Figure 2. Alternative initial steps in the mechanism of reaction between TNT and OH^-.

Prior work on the reaction of DNAN with OH^- is more limited. The reaction between DNAN and OH^- has been suggested to occur through substitution of the methoxy group, leading to 2,4-nitrophenol,[51,52] which may in turn react with OH^- to form 2,4-dinitrophenolate.[52] This reaction may take place through OH^- addition at the C1 carbon (as shown in Figure 3),[51] i.e., through the formation of a Meisenheimer complex. Meisenheimer complex formation at the C1 carbon—as well as at other possible addition sites—is shown in Figure 3 as an initial step in methoxy substitution. In addition, we considered proton abstraction and direct nitro substitution reactions in order to compare the results with those calculated for TNT, although, to our knowledge, these reactions have not been observed experimentally.

Experimental Kinetic Data. In order to provide experimental evidence for evaluating the alternative mechanisms of interaction between TNT and DNAN with OH^-, the disappearance kinetics for these NACs were determined in aqueous phosphate buffer at three pH's (from 11.0 to 12.0) and four temperatures (from 11 to 55 °C for TNT and 25 to 65 °C for DNAN). Representative concentration vs time data are shown in Figure 4 for TNT at 11 °C and DNAN at 25 °C. The complete data set—including additional data for TNT at 25, 40, and 55 °C and for DNAN at 40, 55, and 65 °C—is given in the Supporting Information (SI), Table S1 and Table S3.

For both TNT and DNAN, the kinetics of reaction with OH^- appeared to be first-order with respect to both the NAC and OH^- (second-order overall). TNT disappearance did not

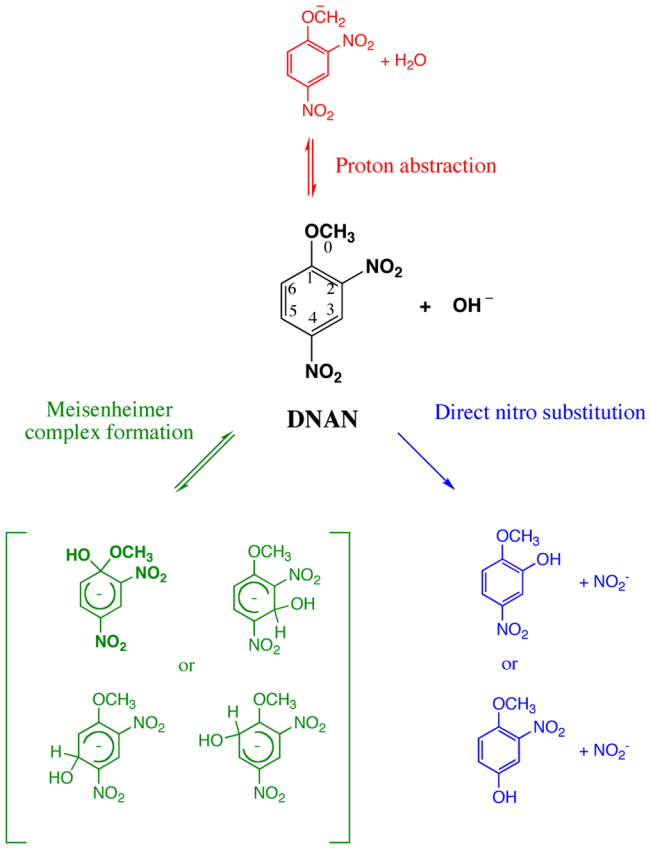

Figure 3. Alternative initial steps in the mechanism of reaction between DNAN and OH^-. Meisenheimer complex formation at C1, which has been hypothesized based on experimental observations,[51] is shown in bold.

show simple, irreversible pseudo-first-order behavior but was better fit to a model that includes a reversible first step, followed by an irreversible second step (as described in Scheme 1 and Scheme 2). A similar model has been used in prior work on the kinetics of intermediate formation upon the reaction of TNT with OH^-.[26] Fitting this model to the data for TNT disappearance gave rate constants for each step, which are summarized in the SI, Table S2. Unlike TNT, the disappearance of DNAN was well fit with a simple model for irreversible, pseudo-first-order kinetics (Scheme 3 and Scheme 4). Rate constants determined from this fit are summarized in the SI, Table S4.

Determination of Free Energies from Experimental Kinetics. To generalize the results obtained from batch experiments with TNT and DNAN and to facilitate comparisons between these results and data obtained from computational modeling (next section), the rate constants for each temperature were used to obtain experimental free energies for the reactions of TNT and DNAN with OH^-. This was done by applying transition state theory,[10] which relates the rate of a reaction to the energy of the transition state, specifically, the free energy of activation ($\Delta G^{\ddagger}$). This relationship is defined by the Eyring equation[10] (eq 4)

$$k = \frac{k_B T}{h} \cdot e^{-\Delta G^{\ddagger}/RT} \cdot (1\ \mathrm{mol\ L^{-1}})^{1-n} \quad (4)$$

where k is the rate constant in molar concentration units (if applicable), k_B is the Boltzmann constant, T is temperature, h is Planck's constant, $\Delta G^{\ddagger}$ is the molar free energy of activation, R

dx.doi.org/10.1021/es304461t | Environ. Sci. Technol. 2013, 47, 6790−6798

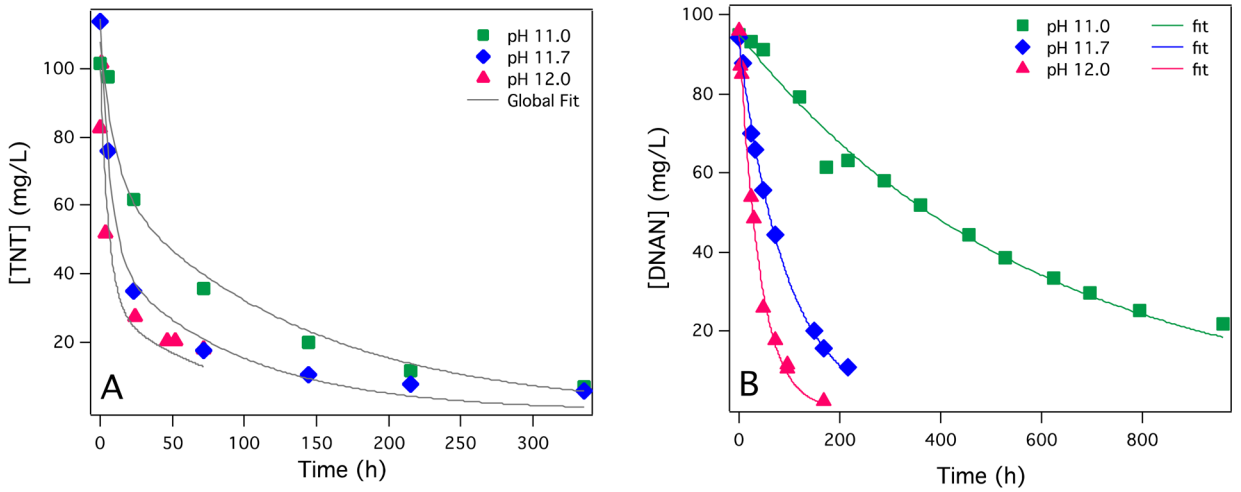

Figure 4. (A) TNT disappearance at 11 °C for pH 11.0, 11.7, and 12.0. All three data sets were fit with constraints that gave global values for k_{-1} and k_2 but separate values for $k_{1,obs}$ at each pH. Data for 25, 40, and 55 °C are shown in the SI, Table S1. (B) DNAN disappearance at 25 °C for pH 11.0, 11.7, and 12.0. Each data set was fit individually to determine $k_{1,obs}$. Data for 40, 55, and 65 °C are shown in the SI, Table S3.

is the gas constant, and n is the order of the reaction. Activation parameters were determined from the rate data using a linearized version of the Eyring equation (eq 5)

$$\ln\left(\frac{k \cdot h}{k_B T (\mathrm{mol\,L^{-1}})^{1-n}}\right) = \frac{\Delta S^{\ddagger}}{R} - \frac{\Delta H^{\ddagger}}{RT} \qquad (5)$$

where $\Delta S^{\ddagger}$ is the molar entropy of activation, and $\Delta H^{\ddagger}$ is the molar enthalpy of activation.

Figure 5 shows Eyring plots for the proposed steps in the reaction of TNT with OH^-, including both the forward and reverse formation of the first product, P1, and subsequent degradation of P1 to P2. The plots show adjusted values of k_1, k_{-1}, and k_2 plotted vs inverse temperature. Also shown in Figure 5 are kinetic data for the reaction of TNT with OH^- previously reported by Mills et al.,[26] who fit their data assuming reversible Meisenheimer-complex formation (using a kinetic model that accounts for reversibility in the initial step), and Emmrich,[22] who obtained k_1 by fitting to an irreversible, pseudo-first-order model.

As seen in Figure 5, our data for k_1 (associated with the reaction TNT + OH^- → P1) show good agreement with those reported previously. In the case of k_{-1} (associated with the reaction TNT + OH^- ← P1), our data does not agree as closely with the data reported by Mills et al.[26] Our data do, however, show a more linear relationship and smaller uncertainties. The reason for the inconsistency between these results is likely that Mills et al. did not consider the effect of the second reaction (P1 → P2) in their determination of k_1 and k_{-1}. They made the assumption that the second reaction does not affect the disappearance of TNT at "low" hydroxide concentrations (0.01−0.1 mol dm^{-3}), and so they used data gathered in this concentration range to study the initial reaction independently. Their kinetics, which were typically measured over two half-lives, fit well to a model based on this assumption. Our data, however, show that the kinetics of TNT disappearance deviate from pseudo-first-order after two half-lives (most of our experiments were run for 4−8 half-lives) and that this deviation is consistent with the contribution of the second reaction (P1 → P2) to the rate of TNT disappearance. For this reason, we fit only our data to eq 5 to determine $\Delta S^{\ddagger}$ and $\Delta H^{\ddagger}$ for each reaction shown in Figure 5. These were subsequently used to calculate $\Delta G^{\ddagger}$ at 25 °C. All of these results are tabulated in Table 1.

In addition to determining activation parameters for the reaction of TNT, a similar treatment was used to extract thermodynamic values from the kinetic data for DNAN. The results are shown in Figure 6 as an Eyring plot for the second-order rate constant, k_1. Error bars on k_1 represent the uncertainties (±1 standard deviation) from the fit of $k_{1,obs}$ vs [OH^-] (SI, Table S1). While the data point corresponding to the experiments performed at 65 °C shows relatively large error, exclusion of this point does not significantly change the value of $\Delta G^{\ddagger}$ calculated from the linear fit. Superimposed on the figure are the rate constants for the reaction of DNAN with OH^- that were reported by Murto and Tommila,[52] which were also obtained by modeling their data with pseudo-first-order kinetics. While their data set shows an essentially identical slope to the result from this study, their intercept is about an order of magnitude smaller (note that, according to the Eyring equation, the slope is related to $\Delta H^{\ddagger}$ and the intercept is related to $\Delta S^{\ddagger}$). Absent any *a priori* explanation for this difference, we have fit each data set to the linearized Eyring equation and reported both sets of results in Table 1. There is no significant difference between the values of $\Delta G^{\ddagger}$ determined from these two data sets.

Determination of Free Energies from Molecular Modeling. In addition to measuring the rate constants and determining free energies for TNT and DNAN experimentally, solution phase reaction energies and activation barriers for the candidate mechanisms shown in Figures 2 and 3 were determined using electronic structure calculations. Data determined at the COSMO B3LYP and COSMO MP2 levels are summarized in Figure 7, which shows ΔG_{rxn} and $\Delta G^{\ddagger}$ vs shorthand labels for each candidate mechanism. This shorthand represents the mechanism ("MC" = Meisenheimer-complex formation, "Sub" = direct nitro substitution, "PA" = proton abstraction) and reaction location (e.g., "@1" = reaction occurring at C1, as labeled in Figures 2 and 3). Also shown are data previously reported by Hill et al.,[34] which were modeled in the solution phase using DFT at the SMD (Pauling)/MO6-2X/6-31+G(d,p) level.[53,54] The values for all the computational results summarized in Figure 7 are given in the SI, Table S5.

dx.doi.org/10.1021/es304461t | *Environ. Sci. Technol.* 2013, 47, 6790−6798

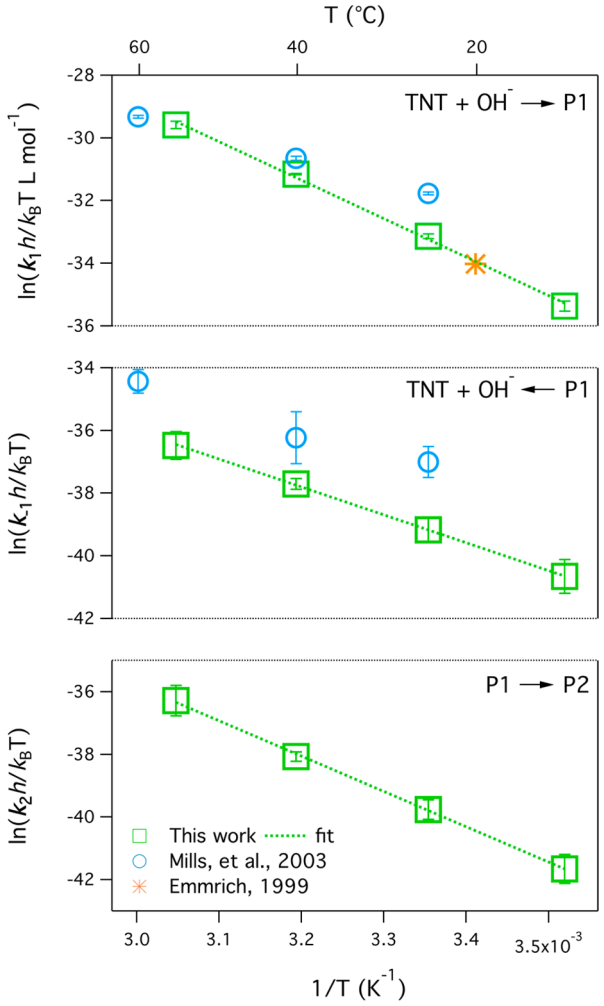

Figure 5. Eyring plots for the reaction of TNT with hydroxide. Each panel in the figure displays rate constants for a different step in the proposed reaction of TNT with OH^- (as described in Scheme 1) according to a linearized version of the Eyring equation (eq 5). The top panel of the figure corresponds to k_1 and the forward portion of the first reaction (TNT + OH^- → P1), the middle panel corresponds to k_{-1} and the reverse portion of the first reaction (TNT + OH^- ← P1), and the bottom panel corresponds to k_2 and the second reaction (P1 → P2). Also shown are data reported by Mills et al.[26] and Emmrich.[22] Error bars are shown for all data, with the exception of the value reported by Emmrich, for which no uncertainty was reported.

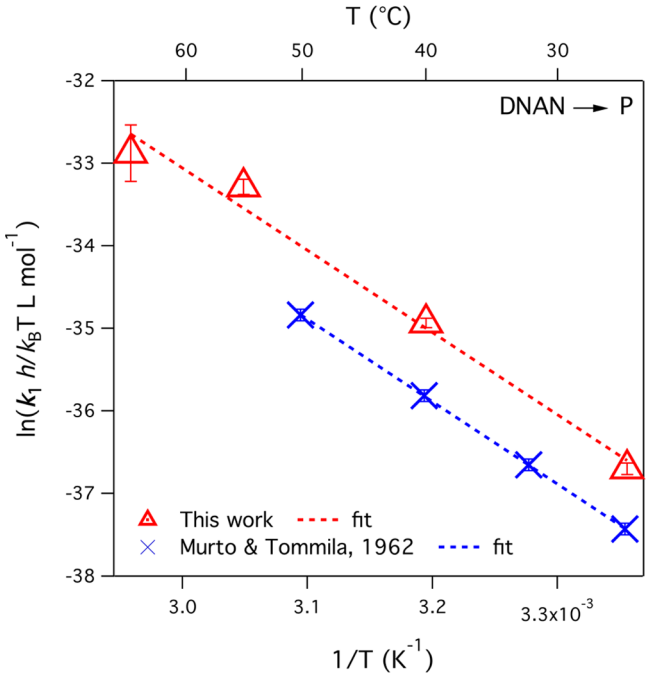

Figure 6. Eyring plot for the reaction of DNAN with hydroxide. A transformation of the second-order rate constant, k_1, is plotted vs inverse temperature (based on a linearized version of the Eyring equation). Data reported in this work are shown as red triangles. Error bars on k_1 represent the error (±1 standard deviation) from the fit of $k_{1,obs}$ vs [OH^-] (SI, Table S1). Data reported by Murto and Tommila[52] are shown as blue ×'s. Each data set was fit linearly to determine Eyring parameters given in Table 1.

In Figure 7, it can be seen that there is considerable variation in the absolute values of ΔG_{rxn} for a given mechanism calculated at different levels of theory (with average absolute differences in ΔG_{rxn} ranging from 5.5 kcal mol^{-1} between the COSMO B3LYP data and the COSMO MP2 data and 11 kcal mol^{-1} between the COSMO B3LYP data and the data reported by Hill et al.). Despite this variation, there is generally good agreement in the relative values of ΔG_{rxn} between the mechanisms, especially between the COSMO B3LYP and COSMO MP2 data. The trends in $\Delta G^{\ddagger}$ are less consistent. The average absolute differences from COSMO B3LYP, however, are slightly smaller than seen for ΔG_{rxn} (5.0 kcal mol^{-1} for COSMO MP2 and 7.2 kcal mol^{-1} for Hill et al.). While our results are not sufficient to determine the absolute accuracy of these calculations (as this was not within the scope of this paper), our ΔG_{rxn} values can be used to determine the relative favorability of each of the candidate mechanisms, and our $\Delta G^{\ddagger}$ values can be used to determine the relative kinetics.

From the ΔG_{rxn} values for both TNT and DNAN shown in Figure 7, it is clear that direct nitro substitution at C2 and C4 (Sub@2 and Sub@4) are the most thermodynamically favorable mechanisms. The ΔG_{rxn} values for TNT at both reaction sites are ~10 kcal mol^{-1} more negative than the analogous reactions on DNAN, suggesting TNT is the more

Table 1. Eyring Fit and Activation Parameters for TNT and DNAN[c]

parent	rxn	Eyring slope (K)	Eyring intercept	$\Delta H^{\ddagger}$ (kcal mol^{-1})	$\Delta S^{\ddagger}$ (kcal K^{-1} mol^{-1})	$\Delta G^{\ddagger a}$ (kcal mol^{-1})
TNT	TNT → P1	−12270 ± 430	7.9 ± 1.4	24.370 ± 0.030	0.01573 ± 0.00051	19.6810 ± 0.0016
TNT	TNT ← P1	−8882 ± 49	−9.38 ± 0.16	17.63866 ± 0.00055	−0.018634 ± 5.5 × 10^{-6}	23.194517 ± 3.1 × 10^{-5}
TNT	P1 → P2	−11282 ± 97	−1.95 ± 0.32	22.4061 ± 0.0017	−0.00388 ± 0.00010	23.56230 ± 0.00073
DNAN	DNAN → P	−9960 ± 870	−3.2 ± 2.7	19.79 ± 0.15	−0.0063 ± 0.0046	21.66 ± 0.54
		−9986 ± 32[b]	−3.9324 ± 0.10[b]	19.83200 ± 2.0 × 10^{-4}[b]	−0.0078097 ± −5.4 × 10^{-6}[b]	22.160473 ± 1.0 × 10^{-5}[b]

[a]Calculated at 25 °C from $\Delta H^{\ddagger}$ and $\Delta S^{\ddagger}$. [b]Determined by fitting data reported by Murto and Tommila.[52] [c]Except where indicated, all parameters reported were determined by fitting data original to this work.

dx.doi.org/10.1021/es304461t | Environ. Sci. Technol. 2013, 47, 6790−6798

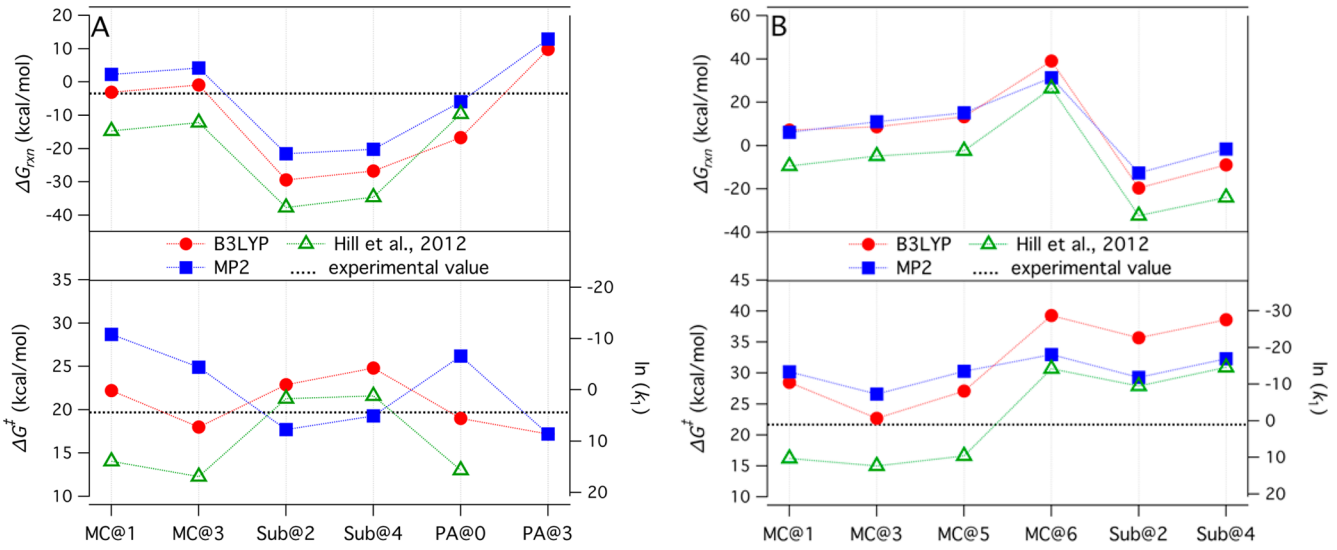

Figure 7. Computationally determined reaction free energies (ΔG_{rxn}) and activation free energies ($\Delta G^{\ddagger}$) for (A) TNT and (B) DNAN. Values are shown for the possible initial reaction steps determined at the COSMO B3LYP and COSMO MP2 levels. Also shown are data reported by Hill et al.[34] Experimentally determined values (derived from fits to the kinetic results) are shown as black dotted lines.

favorable of the two. This is easily rationalized by the additional electron-withdrawing group on TNT. The $\Delta G^{\ddagger}$ values for Sub@2 and Sub@4 show a similar trend to the ΔG_{rxn} values, with the $\Delta G^{\ddagger}$ values for TNT being ~10 kcal mol^{-1} lower than the values for DNAN. The high values of $\Delta G^{\ddagger}$ for DNAN suggest that the reactions should occur more slowly than for TNT and are not likely to be kinetically significant.

Compared to direct nitro substitution, the ΔG_{rxn} values for Meisenheimer-complex formation and proton abstraction are less favorable for both TNT and DNAN. ΔG_{rxn} values for Meisenheimer-complex formation at all sites are near zero for TNT and endothermic by at least 6 kcal mol^{-1} for DNAN. Proton abstraction at the methyl group (PA@0) on TNT is between −20 and 0 kcal mol^{-1} and PA@3 is endothermic by about 10 kcal mol^{-1}. Proton abstraction reactions on DNAN are also endothermic and not thermodynamically feasible (results not shown).

Overall, the computational results predict that TNT can undergo direct substitution (Sub@2 and Sub@4), Meisenheimer-compex formation (MC@1 and MC@3), and proton abstraction at the methyl group (PA@0). For DNAN, the computational results suggest that the direct substitution reactions, while thermodynamically feasible, are not likely because of their high activation barriers, and that only MC@1 and MC@3 are kinetically and thermodynamically favorable.

Reconciling the Computational Results with Experimental Observations. The likelihood of the candidate mechanisms can be further evaluated by comparing the results of molecular modeling to experimental observations. Ideally, this might be based on a comparison of computationally derived ΔG_{rxn} and $\Delta G^{\ddagger}$ values to those determined experimentally in order to determine likely mechanisms. To facilitate such a comparison, Figure 7 has been annotated with experimental values of $\Delta G^{\ddagger}$ for TNT and DNAN and an experimental value of ΔG_{rxn} for TNT. The experimental ΔG_{rxn} was determined from the difference in the experimental $\Delta G^{\ddagger}$ values for the forward and reverse steps in the reaction of TNT with OH^{-}. This calculation could not be performed for DNAN since the initial step in the reaction with OH^{-} was not reversible. As seen in Figure 7, however, different levels of theory produce a substantial range of computed values of $\Delta G^{\ddagger}$. Because of this variability, and because there is no way to know a priori which level of theory best reflects experimental observations, we have not made a direct comparison of the computational and experimental values for ΔG_{rxn} and $\Delta G^{\ddagger}$. Other comparisons can be made, however, which lead to a number of significant conclusions.

In the case of TNT, kinetic modeling of the experimental results, shown in Figure 4 (and in the SI, Tables S1 and S3), suggests a reversible reaction. Assuming reversibility, the ΔG_{rxn} value is expected to be close to 0 kcal mol^{-1} (due to the forward and reverse reactions having similar values of $\Delta G^{\ddagger}$). This is consistent with the experimental ΔG_{rxn} value of −3.5 kcal mol^{-1}. Since the computed ΔG_{rxn} values for Sub@2 and Sub@4 are approximately −25 to −30 kcal mol^{-1}, these mechanisms are likely too favorable to exhibit reversibility. The ΔG_{rxn} values for MC@1, MC@3, PA@0, and PA@3 are more consistent with a reversible reaction.

Based on these considerations and the analysis given in the previous section, MC@1, MC@3, and PA@0 appear to be the most likely initial steps in the reaction between TNT and OH^{-} in water. Of these, the mechanisms that show the closest agreement between the computed value of $\Delta G^{\ddagger}$ (at both the COMSO B3LYP and COSMO MP2 levels) and the experimental value are MC@3 and PA@0. However, as mentioned previously, we do not know *a priori* how accurate the computational methods are. Additionally, the value of $\Delta S^{\ddagger}$ determined from the fit of the TNT disappearance data (Table 1) is positive, suggesting that the transition state shows increased disorder compared to TNT. This implies a dissociative mechanism such as proton abstraction. Therefore, given the overall uncertainty in the results, we cannot conclude which mechanism (MC@1, MC@3, or PA@0) predominates or if the observed kinetics reflect a combination of mechanisms.

In the case of DNAN, the computational and experimental results are not as consistent regarding the reversibility or irreversibility of the reaction. The experimental kinetics suggest an irreversible reaction, for which a ΔG_{rxn} much lower than 0 kcal mol^{-1} (generally less than about −20 kcal mol^{-1}) is expected. However as seen in Figure 7, MC@1 and MC@3,

dx.doi.org/10.1021/es304461t | Environ. Sci. Technol. 2013, 47, 6790−6798

which are the top candidate mechanisms based on the analysis given in the previous section, have slightly positive ΔG_{rxn} values. While the reason for this discrepancy is uncertain, possible explanations are either that (i) there is another pathway not considered here that has a lower $\Delta G^{\ddagger}$ and is exothermic, or (ii) the theory is not accurately describing the transition states of this pathway, perhaps due to the fact that the continuum solvation model is overestimating the first transition state because it is nearly dissociated. While other pathways are possible, MC@1 is a very likely initial reaction, based on the previously observed products of the reaction, 2,4-dinitophenol[51,52] and, subsequently, 2,4-dinitrophenolate.[52] Additionally, molecular modeling of the pathway between DNAN and 2,4-dinitrophenolate at the COSMO B3LYP and COSMO MP2 levels predicts MC@1 to be the initial step of the reaction (details are reported in the SI, Figure S1).

Previous efforts have failed to unambiguously define mechanisms for the reactions of TNT and DNAN with OH^-, especially in the case of TNT where product characterization has been particularly challenging. The experimental and computational observations reported here provide insight into these mechanisms, although some ambiguity remains, especially in the case of TNT. Because of this ambiguity, it is uncertain whether TNT and DNAN react by the same mechanism. The possible difference in mechanisms means that predicting the reaction mechanism for one based on the other may lead to unreliable predictions of environmental fate. This, along with uncertainties in the consistency of the calculated results with experimental values presents a challenge for developing QSARs calibrated "fully *in silico*" that predict the hydrolysis behavior of the diverse range of energetic NACs.

■ ASSOCIATED CONTENT

Supporting Information

Summaries of the kinetic data collected and detailed molecular modeling results. This material is available free of charge via the Internet at http://pubs.acs.org.

■ AUTHOR INFORMATION

Corresponding Author

*Phone: 503-748-1023; fax: 503-748-1464; e-mail: tratnyek@ebs.ogi.edu.

Notes

The authors declare no competing financial interest.

■ ACKNOWLEDGMENTS

This work was supported by the Strategic Environmental Research and Development Program (SERDP) under ER1735. This report has not been subject to review by SERDP and therefore does not necessarily reflect their views and no official endorsement should be inferred. A portion of this research was performed using the PNNL Institutional Computing (PIC) facility and the Chinook and Spokane computing resources at the Molecular Science Computing Facility at EMSL, a national scientific user facility sponsored by the Department of Energy's Office of Biological and Environmental Research located at Pacific Northwest National Laboratory, DE-AC06-76RLO 1830. We also acknowledge EMSL for supporting the development of NWChem. The Pacific Northwest National Laboratory is operated by Battelle Memorial Institute. Structure database management and sorting was performed using Instant JChem (Instant JChem 5.9, 2011, ChemAxon [http://www.chemaxon.com]).

■ REFERENCES

(1) Talmage, S.; Opresko, D.; Maxwell, C.; Welsh, C.; Cretella, F.; Reno, P.; Daniel, F. Nitroaromatic munition compounds: Environmental effects and screening values. *Rev. Environ. Contam. Toxicol.* **1999**, *161*, 1−156.

(2) Juhasz, A. L.; Naidu, R. Explosives: Fate, dynamics, and ecological impact in terrestrial and marine environments. *Rev. Environ. Contam. Toxicol.* **2007**, *191*, 163−215.

(3) Anastas, P. T.; Warner, J. C. *Green Chemistry: Theory and Practice*; Oxford University Press: USA, 2000.

(4) Talawar, M.; Sivabalan, R.; Mukundan, T.; Muthurajan, H.; Sikder, A.; Gandhe, B.; Rao, A. Environmentally compatible next generation green energetic materials (GEMs). *J. Hazard. Mater.* **2009**, *161*, 589−607.

(5) Huynh, M.; Hiskey, M.; Meyer, T.; Wetzler, M. Green primaries: Environmentally friendly energetic complexes. *Proc. Natl. Acad. Sci. (USA)* **2006**, *103*, 5409−5412.

(6) Walker, J. QSARS promote more efficient use of chemical testing resources - Carpe diem. *Environ. Toxicol. Chem.* **2003**, *22*, 1651−1652.

(7) Donaldson, W. T. The role of property-reactivity relationships in meeting the EPA's needs for environmental fate constants. *Environ. Toxicol. Chem.* **1992**, *11*, 887−891.

(8) Mackay, D.; Webster, E. A perspective on environmental models and QSARs. *SAR QSAR Environ. Res.* **2003**, *14*, 7−16.

(9) Tratnyek, P.; Weber, E.; Schwarzenbach, R. Quantitative structure-activity relationships for chemical reductions of organic contaminants. *Environ. Toxicol. Chem.* **2003**, *22*, 1733−1742.

(10) Maskill, H. *The Physical Basis of Organic Chemistry*; Oxford Science Publications: Oxford, 1989.

(11) Gray, N. *Army AL&T* **2008**, 34−35.

(12) Chow, T. M.; Wilcoxon, M. R.; Piwoni, M. D.; Maloney, S. W. Analysis of new generation explosives in the presence of US EPA Method 8330 energetic compounds by high-performance liquid chromatography. *J. Chromatogr. Sci.* **2009**, *47*, 40−43.

(13) Sikder, A.; Sikder, N. A review of advanced high performance, insensitive and thermally stable energetic materials emerging for military and space applications. *J. Hazard. Mater.* **2004**, *112*, 1−15.

(14) Millar, R. W.; Hamid, J.; Endsor, R.; Swinton, P. F.; Cooper, J. Selection and synthesis of energetic heterocyclic compounds suitable for use in insensitive explosive and propellant compositions. *Propellants, Explos., Pyrotech.* **2008**, *33*, 66−72.

(15) Monteil-Rivera, F.; Halasz, A.; Groom, C.; Zhao, J.-S.; Thiboutot, S.; Ampleman, G.; Hawari, J. Fate and transport of explosives in the environment: A chemist's view. In *Ecotoxicology of Explosives*; Sunahara, G. I., Lotufo, G., Kuperman, R. G., Hawari, J., Eds.; CRC Press: Boca Raton, FL, 2009; 5−33.

(16) Schwarzenbach, R.; Stierli, R.; Lanz, K.; Zeyer, J. Quinone and iron porphyrin mediated reduction of nitroaromatic compounds in homogeneous aqueous solution. *Environ. Sci. Technol.* **1990**, *24*, 1566−1574.

(17) Hofstetter, T.; Heijman, C.; Haderlein, S.; Holliger, C.; Schwarzenbach, R. Complete reduction of TNT and other (poly)-nitroaromatic compounds under iron-reducing subsurface conditions. *Environ. Sci. Technol.* **1999**, *33*, 1479−1487.

(18) Hartenbach, A.; Hofstetter, T.; Berg, M.; Bolotin, J.; Schwarzenbach, R. Using nitrogen isotope fractionation to assess abiotic reduction of nitroaromatic compounds. *Environ. Sci. Technol.* **2006**, *40*, 7710−7716.

(19) Hartenbach, A.; Hofstetter, T.; Aeschbacher, M.; Sander, M.; Kim, D.; Strathmann, T. J.; Arnold, W.; Cramer, C.; Schwarzenbach, R. Variability of nitrogen isotope fractionation during the reduction of nitroaromatic compounds with dissolved reductants. *Environ. Sci. Technol.* **2008**, *42*, 8352−8359.

(20) Strathmann, T. J. Redox reactivity of organically complexed iron(II) species with aquatic contaminants. In *Aquatic Redox Chemistry*; Tratnyek, P. G., Grundl, T. J., Haderlein, S. B., Eds.;

American Chemical Society: Washington, DC, 2011; ACS Symp. Ser. No. 1071, pp 283−313.
(21) Saupe, A.; Garvens, H.; Heinze, L. Alkaline hydrolysis of TNT and TNT in soil followed by thermal treatment of the hydrolysates. *Chemosphere* **1998**, *36*, 1725−1744.
(22) Emmrich, M. Kinetics of the alkaline hydrolysis of 2,4,6-trinitrotoluene in aqueous solution and highly contaminated soils. *Environ. Sci. Technol.* **1999**, *33*, 3802−3805.
(23) Emmrich, M. Kinetics of the alkaline hydrolysis of important nitroaromatic co-contaminants of 2,4,6-trinitrotoluene in highly contaminated soils. *Environ. Sci. Technol.* **2001**, *35*, 874−877.
(24) Karasch, C.; Popovic, M.; Qasim, M.; Bajpai, R. Alkali hydrolysis of trinitrotoluene. *Appl. Biochem. Biotechnol.* **2002**, *98*−*100*, 1173−1185.
(25) Felt, D.; Larson, S.; Valente, E. UV-VIS spectroscopy of 2,4,6-trinitrotoluene-hydroxide reaction. *Chemosphere* **2002**, *49*, 287−295.
(26) Mills, A.; Seth, A.; Peters, G. Alkaline hydrolysis of trinitrotoluene, TNT. *Phys. Chem. Chem. Phys.* **2003**, *5*, 3921−3927.
(27) Thorn, K.; Thorne, P.; Cox, L. Alkaline hydrolysis/polymerization of 2,4,6-trinitrotoluene: Characterization of products by ^{13}C and ^{15}N NMR. *Environ. Sci. Technol.* **2004**, *38*, 2224−2231.
(28) Bajpai, R.; Parekh, D.; Herrmann, S.; Popović, M.; Paca, J.; Qasim, M. A kinetic model of aqueous-phase alkali hydrolysis of 2,4,6-trinitrotoluene. *J. Hazard. Mater.* **2004**, *106*, 55−66.
(29) Felt, D. R.; Larson, S. L.; Hansen, L. D. *Molecular weight distribution of the final products of TNT-hydroxide reaction. ERDC/EL TR-01-16*; U.S. Army Research and Development Center: Vicksburg, MS, 2001.
(30) Davis, J. L.; Nestler, C.; Felt, D. R.; Larson, S. L. *Effect of Treatment pH on the End Products of the Alkaline Hydrolysis of TNT and RDX. ERDC/EL TR-07-4*; U.S. Army Research and Development Center: Vicksburg, MS, 2007.
(31) Felt, D. R.; Nestler, C. C.; Davis, J. L.; Larson, S. L. *Potential for Biodegradation of the Alkaline Hydrolysis End Products of TNT and RDX. ERDC/EL TR-07-25*; U.S. Army Research and Development Center: Vicksburg, MS, 2007.
(32) Bernasconi, C. Kinetic and spectral study of some reactions of 2,4,6-trinitrotoluene in basic solution. I. Deprotonation and Janovsky complex formation. *J. Org. Chem.* **1971**, *36*, 1671−1679.
(33) Fyfe, C.; Malkiewich, C.; Damji, S.; Norris, A. Flow nuclear magnetic resonance investigation of the transient and stable species formed by the attack of alkoxide ions on 2,4,6-trinitrotoluene. *J. Am. Chem. Soc.* **1976**, *98*, 6983−6988.
(34) Hill, F. C.; Sviatenko, L. K.; Gorb, L.; Okovytyy, S. I.; Blaustein, G. S.; Leszczynski, J. DFT M06-2X investigation of alkaline hydrolysis of nitroaromatic compounds. *Chemosphere* **2012**, *88*, 635−643.
(35) Qasim, M. M.; Moore, B.; Taylor, L.; Honea, P.; Gorb, L.; Leszczynski, J. Structural characteristics and reactivity relationships of nitroaromatic and nitramine explosives − A review of our computational chemistry and spectroscopic research. *Int. J. Mol. Sci.* **2007**, *8*, 1234−1264.
(36) Qasim, M.; Gorb, L.; Magers, D.; Honea, P.; Leszczynski, J.; Moore, B.; Taylor, L.; Middleton, M. Structure and reactivity of TNT and related species: Application of spectroscopic approaches and quantum-chemical approximations toward understanding transformation mechanisms. *J. Hazard. Mater.* **2009**, *167*, 154−163.
(37) Valiev, M.; Bylaska, E. J.; Govind, N.; Kowalski, K.; Straatsma, T. P.; Van Dam, H. J. J.; Wang, D.; Nieplocha, J.; Aprà, E.; Windus, T. L.; de Jong, W. A. NWChem: A comprehensive and scalable open-source solution for large scale molecular simulations. *Comput. Phys. Commun.* **2010**, *181*, 1477−1489.
(38) Hohenberg, P.; Kohn, W. Inhomogeneous electron gas. *Phys. Rev. B* **1964**, *136*, 864−871.
(39) Lee, C.; Yang, W.; Parr, R. G. Development of the Colle-Salvetti correlation-energy formula into a functional of the electron density. *Phys. Rev. B* **1988**, *37*, 785.
(40) Becke, A. D. Density-functional thermochemistry. III. The role of exact exchange. *J. Chem. Phys.* **1993**, *98*, 5648.
(41) Møller, C.; Plesset, M. S. Note on an approximation treatment for many-electron systems. *Phys. Rev.* **1934**, *46*, 618−622.
(42) Feller, D.; Schuchardt, K. *Extensible Computational Chemistry Environment Basis Set Database, Version 9/12/01*; Molecular Science Computing Facility, Environmental and Molecular Sciences Laboratory, Pacific Northwest Laboratory: Richland, Washington, USA, 2001.
(43) Klamt, A.; Schüürmann, G. COSMO: A new approach to dielectric screening in solvents with explicit expressions for the screening energy and its gradient. *J. Chem Soc., Perkin Trans. 2* **1993**, *1993*, 799−805.
(44) Stefanovich, E. V.; Truong, T. N. Optimized atomic radii for quantum dielectric continuum solvation models. *Chem. Phys. Lett.* **1995**, *244*, 65−74.
(45) Sitkoff, D.; Sharp, K. A.; Honig, B. Accurate calculation of hydration free energies using macroscopic solvent models. *J. Phys. Chem.* **1994**, *98*, 1978−1988.
(46) Ben-Naim, A.; Marcus, Y. J. Solvation thermodynamics of nonionic solutes. *J. Chem. Phys.* **1984**, *81*, 2016−2016.
(47) Buncel, E.; Norris, A.; Russell, K. The interaction of aromatic nitro-compounds with bases. *Q. Rev. Chem. Soc.* **1968**, *22*, 123−146.
(48) Terrier, F. Rate and equilibrium studies in Jackson-Meisenheimer complexes. *Chem. Rev.* **1982**, *82*, 77−152.
(49) Bruckner, R. *Advanced Organic Chemistry: Reaction Mechanisms*; Hardcourt/Academic Press: 2002.
(50) Urbański, T. *Chemistry and Technology of Explosives*; The Macmillan Company: New York, 1964; Vol. *1*.
(51) Rochester, C. H. Correlation of reaction rates with acidity functions in strongly basic media. *Trans. Faraday Soc.* **1963**, *59*.
(52) Murto, J.; Tommila, E. The influence of the solvent on reaction velocity XXI. The reaction of 2,4-dinitropheyl alkyl ethers with hydroyl ion in water and in methanol-water and ethanol-water mixtures. *Acta Chem. Scand.* **1962**, 63−70.
(53) Kelly, C. P.; Cramer, C. J.; Truhlar, D. G. SM6: A Density functional theory continuum solvation model for calculating aqueous solvation free energies of neutrals, ions, and solute−water clusters. *Acc. Chem. Res.* **2005**, *1*, 1133−1152.
(54) Zhao, Y.; Truhlar, D. G. Density functionals with broad applicability in chemistry. *Acc. Chem. Res.* **2008**, *41*, 157−167.